Electronic Supplementary Information

Ultrafine ZnSe/CoSe Nanodots Encapsulated in Core-shell MOFs-Derived Hierarchically Porous N-doped Carbon Nanotubes for Superior Lithium/Sodium Storage

Qiang Zhang[a], Meng-Li Chen[a], Jin Wang[b], Chen-Fan Zhao[a], Fu-Hu Cao[a], Hao Li[c], Huai-Ping Cong[a], and Chuan-Ling Zhang*[a]

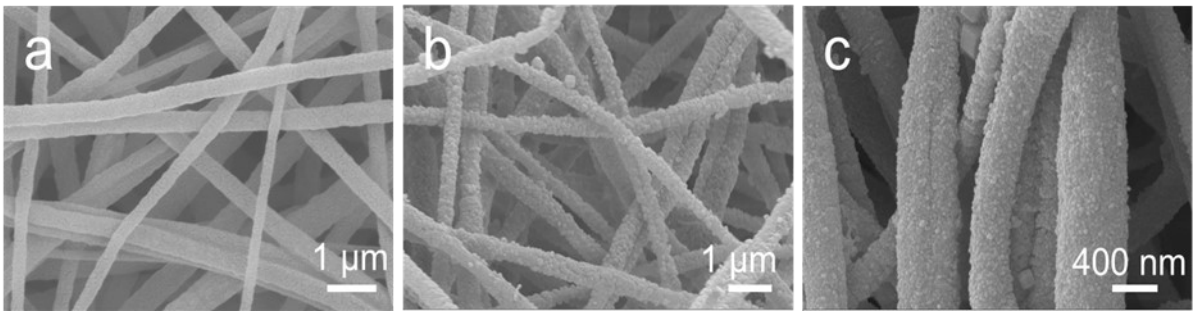

Figure S1. SEM images of **(a)** ES-Zn$(CH_3COO)_2$, **(b)** PAN@ZIF-8, and **(c)** PAN@ZIF-8@ZIF-67, respectively.

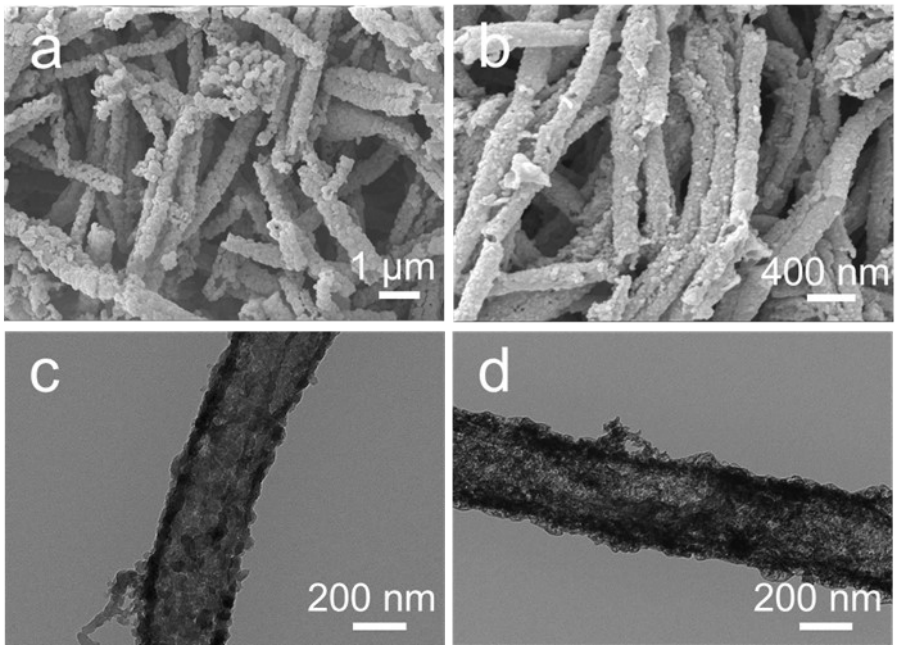

Figure S2. SEM and TEM images of **(a, c)** ZIF-8@ZIF-67 and **(b, d)** ZnSe@CoSe.

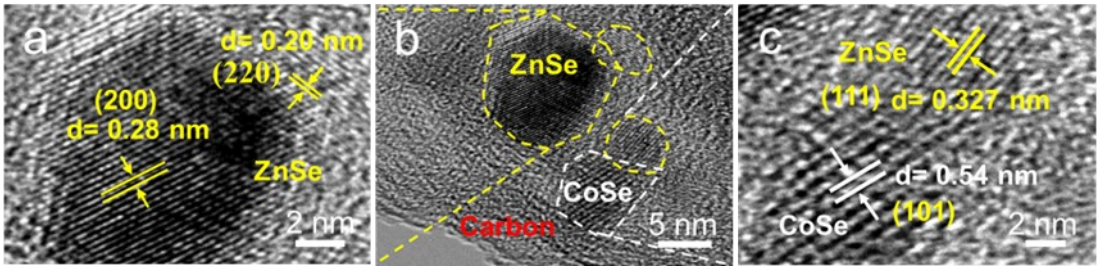

Figure S3. HRTEM images of ZnSe@CoSe@CN.

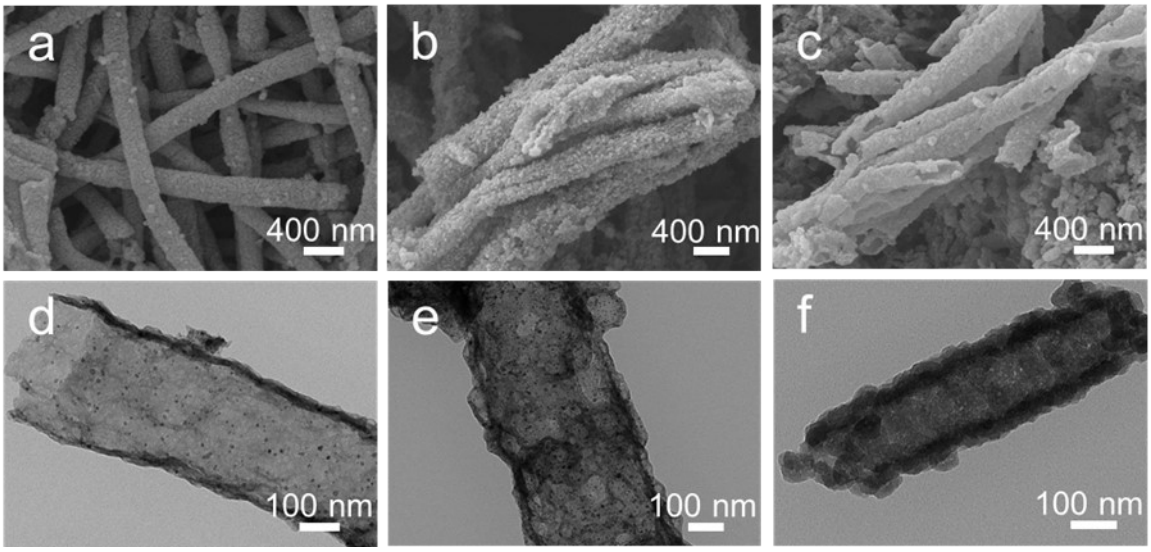

Figure S4. SEM and TEM images of **(a, d)** ZnSe@CN, **(b, e)** CoSe@CN, and **(c, f)** Zn@Co@CN, respectively.

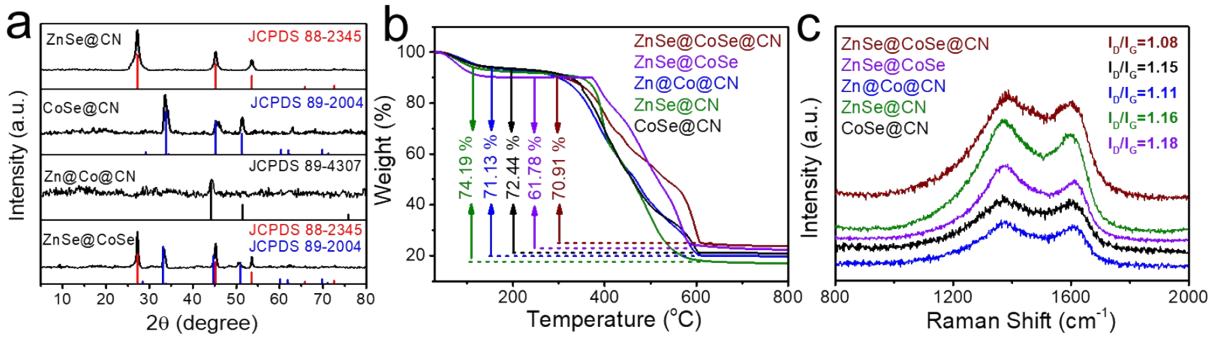

Figure S5. (a) Powder XRD patterns, **(b)** TGA curves, and **(c)** Raman spectra of the samples, respectively.

The TGA curves were characterized under the air atmosphere with the temperature ranging from 30 to 800 °C at a heating rate of 10 °C min^{-1}. It can be observed that when the temperature range was between 30 and 200 °C, the samples have initial marginal weight loss, which is due to the evaporation of free water and physically adsorbed water in the material during the temperature rise, resulting in the quality reduction. Besides, there is a slight mass increase at about 270 °C, which is due to the presence of SeO_2 during the phase transition from selenide to oxide in the material, as shown below:

$$2ZnSe(s) + O_2(g) = 2ZnO(s) + SeO_2(g)$$

$$3CoSe_2(s) + 8O_2(g) = Co_3O_4(s) + 6SeO_2(g)$$

Finally, the severe mass loss of materials from 300 °C to 600 °C can be attributed to the reaction of N-doped carbonaceous components with oxygen, the generation of carbon dioxide gas, and the evaporation of the formed SeO_2 at lower temperatures. According to the above formula and the mass loss, the contents of the N-doped carbon in the samples of ZnSe@CoSe@CN, ZnSe@CN, CoSe@CN, Zn@Co@CN, and ZnSe@CoSe were 70.91%, 74.19%, 72.44%, 56.66%, and 61.76%, respectively.

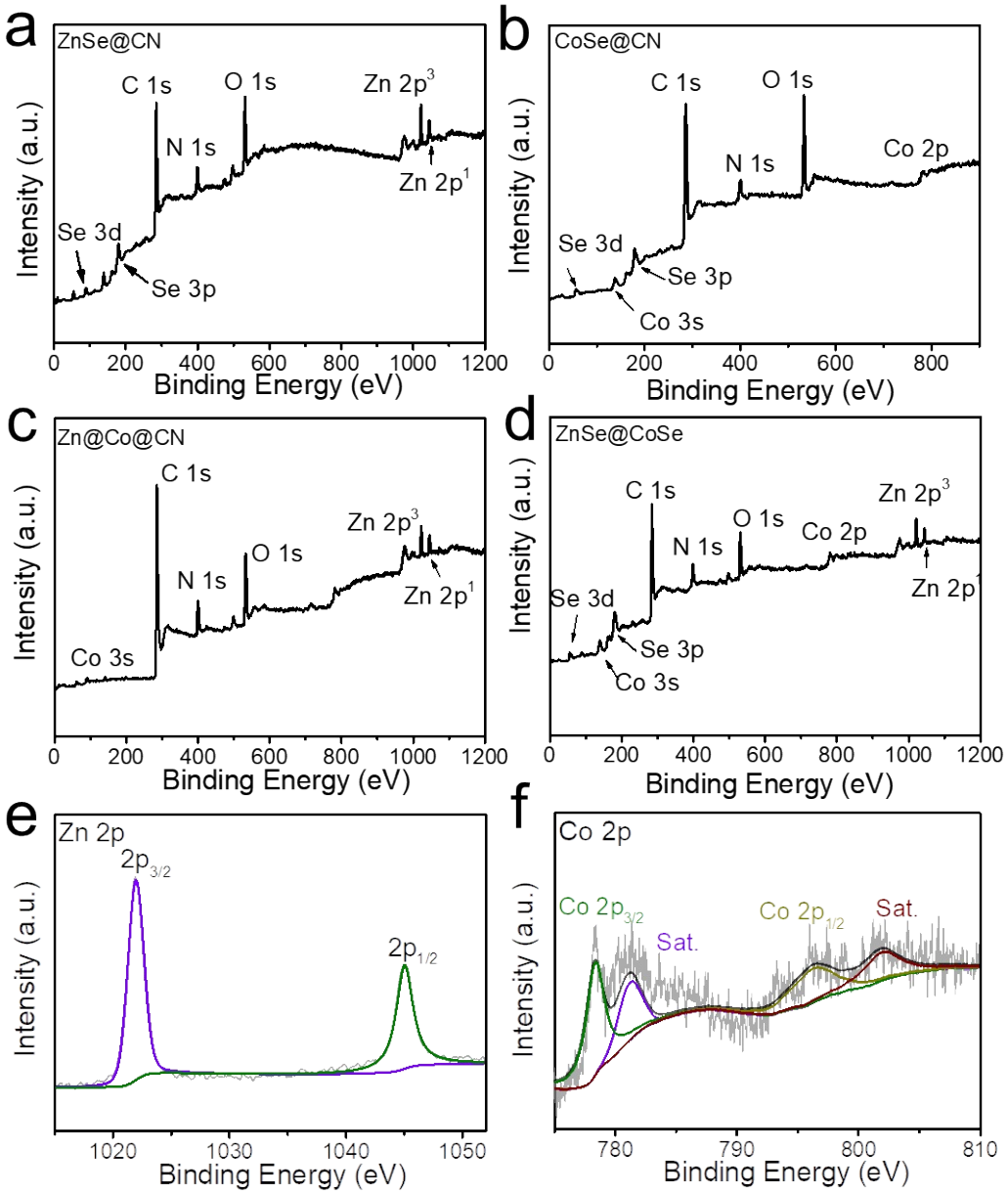

Figure S6. XPS survey spectra of **(a)** ZnSe@CN, **(b)** CoSe@CN, **(c)** Zn@Co@CN, and **(d)** ZnSe@CoSe, respectively. High-resolution XPS spectra of **(e)** Zn 2p of ZnSe@CN and **(f)** Co 2p of CoSe@CN.

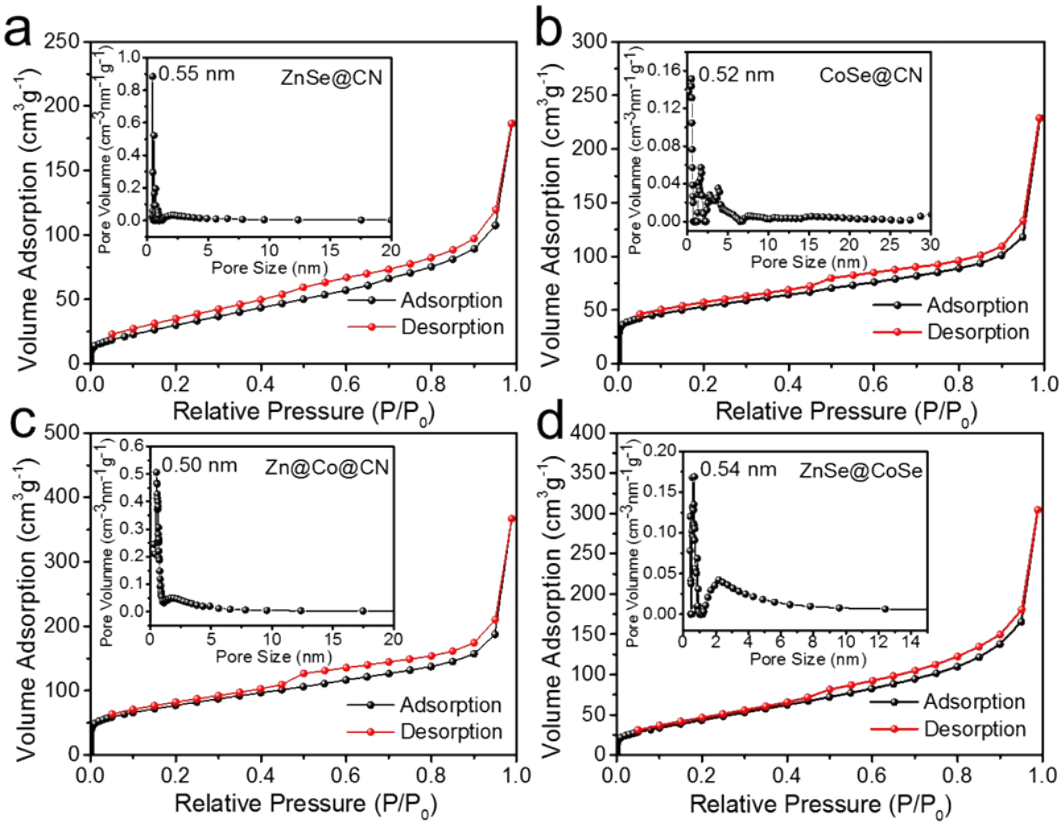

Figure S7. N_2 sorption isotherms of **(a)** ZnSe@CN, **(b)** CoSe@CN, **(c)** Zn@Co@CN, and **(d)** ZnSe@CoSe, respectively. Inset is the corresponding pore size distribution.

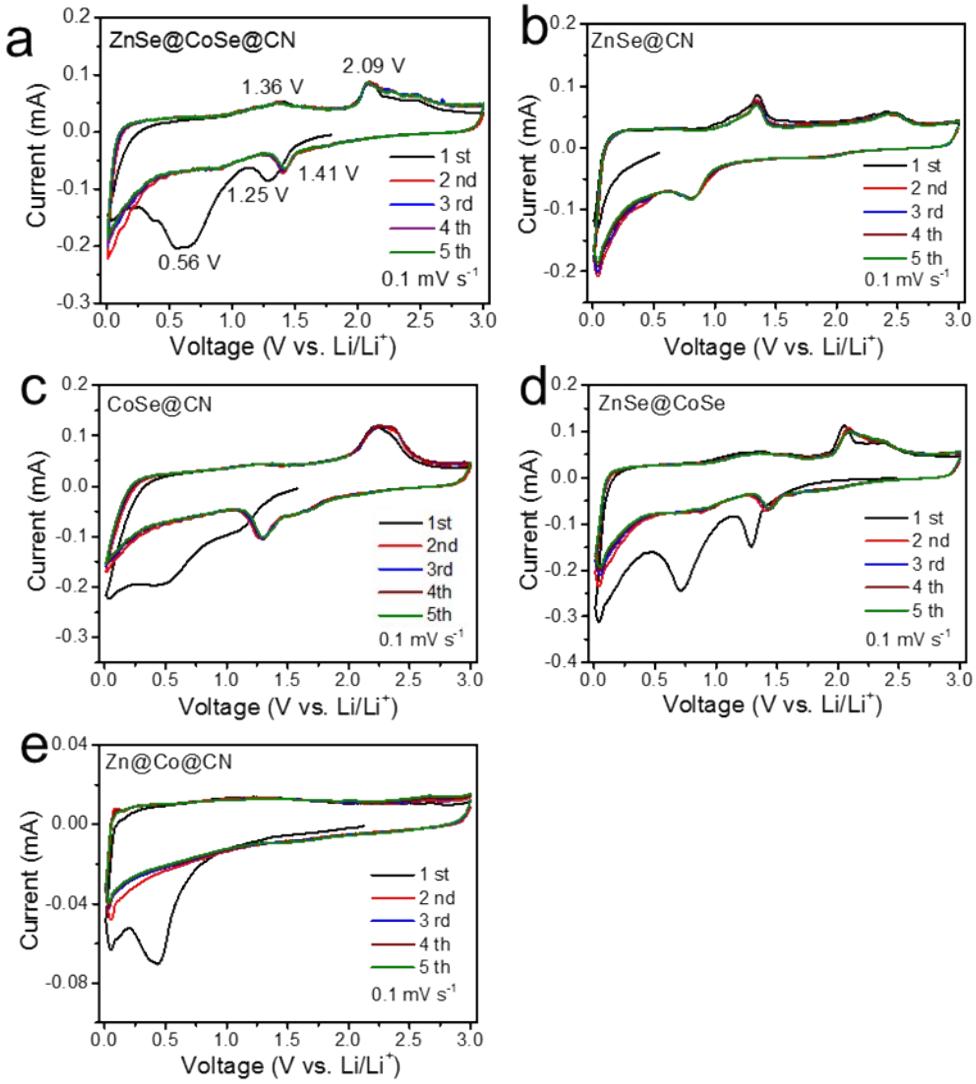

Figure S8. CV profiles of the anodes with a scanning rate of 0.1 mV s^{-1} for lithium-ion storage.

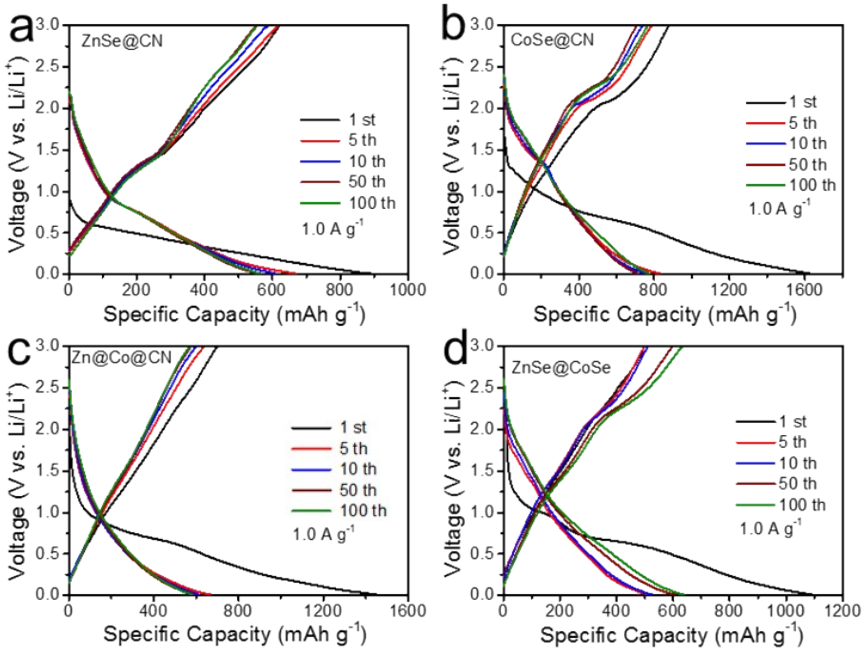

Figure S9. GDC profiles of the contrast anodes at 1.0 A g^{-1} for lithium-ion storage.

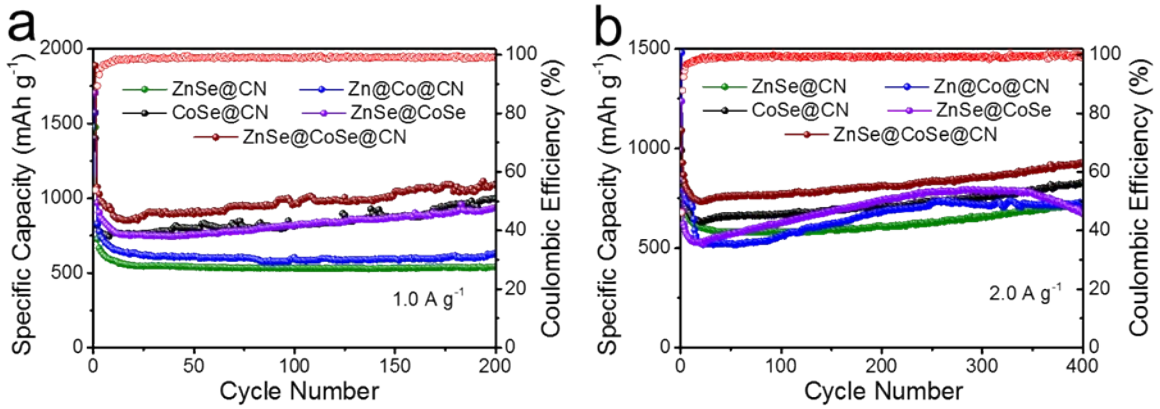

Figure S10. Cycling performance of the anodes at (a) 1.0 A g^{-1} and (b) 2.0 A g^{-1} for lithium-ion storage.

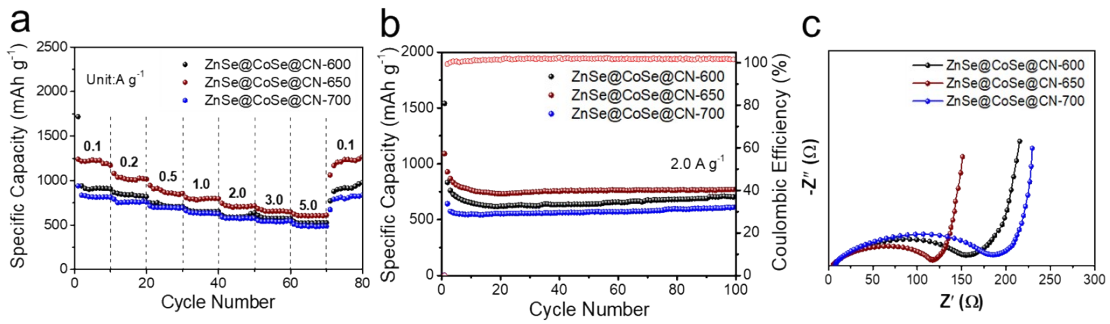

Figure S11. (a) Rate performance, (b) cycling performance, and (c) Nyquist plots of the ZnSe@CoSe@CN anodes prepared at different pyrolysis temperatures for lithium-ion storage.

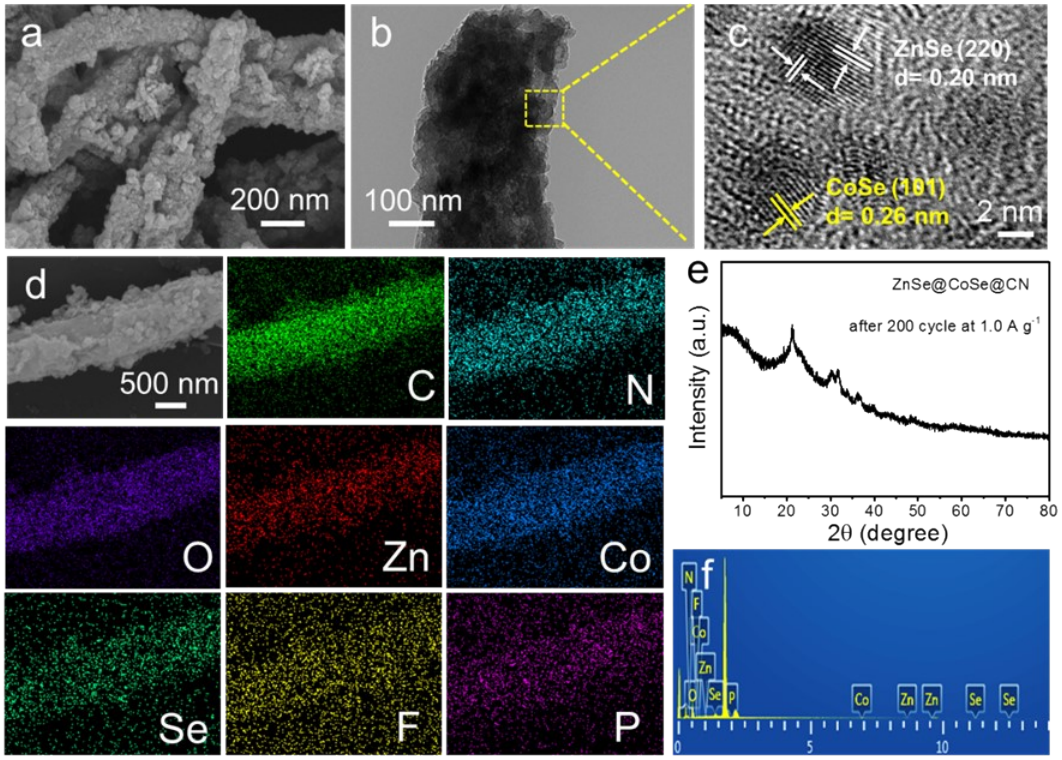

Figure S12. (a) SEM, (b) TEM, (c) HRTEM, (d) elemental mapping images, (e) XRD pattern, and (f) EDS pattern of the ZnSe@CoSe@CN anode after 200 cycles at 1.0 A g^{-1}, respectively.

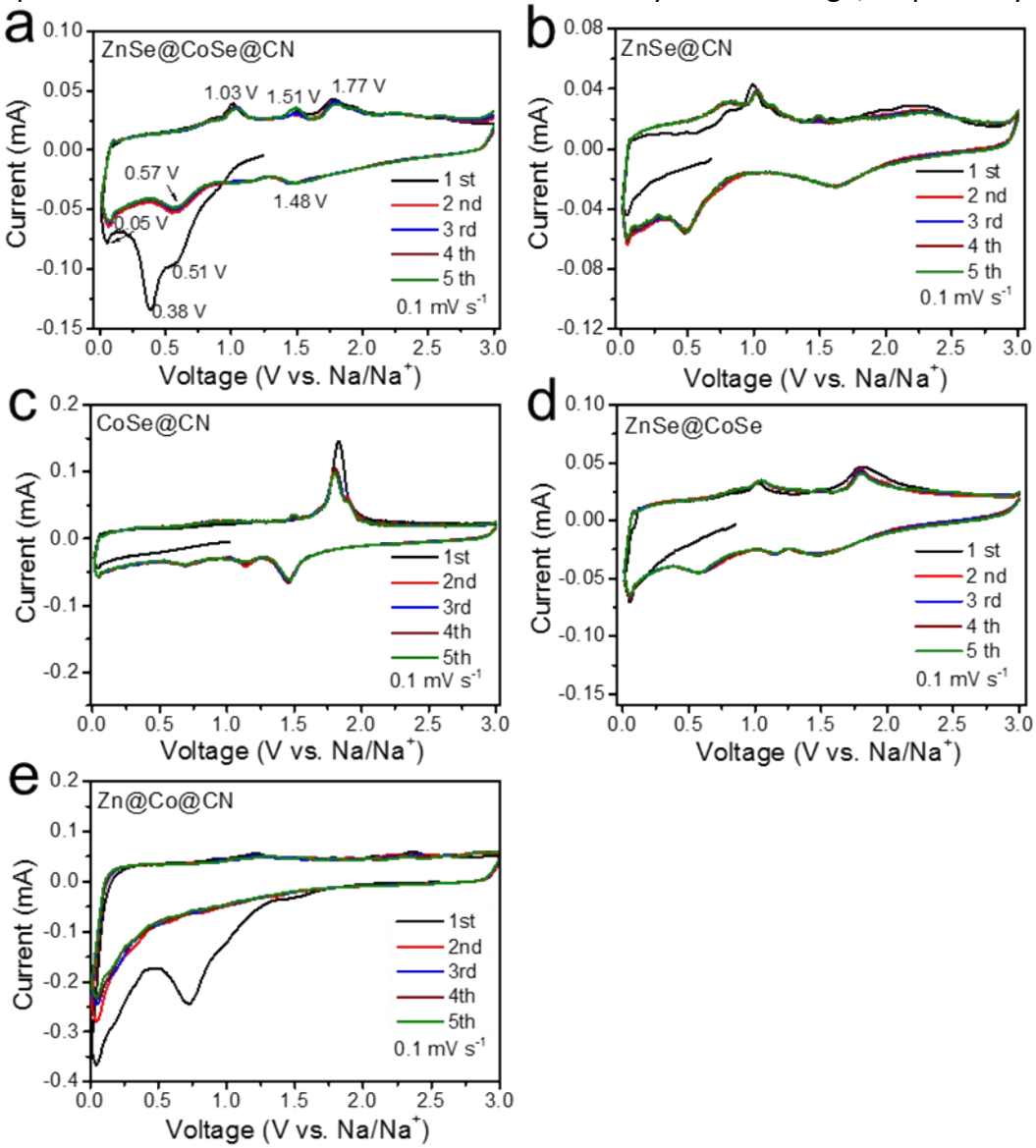

Figure S13. CV profiles of the anodes with a scanning rate of 0.1 mV s^{-1} for sodium-ion storage.

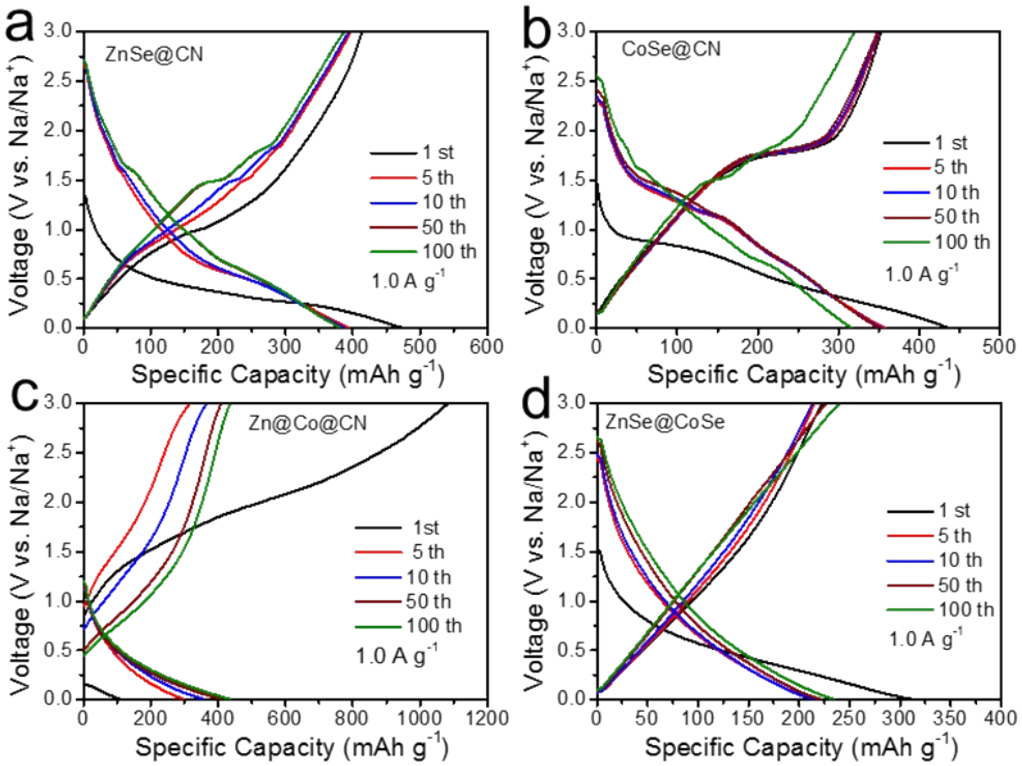

Figure S14. GDC profiles of (a) ZnSe@CN, (b) CoSe@CN, (c) Zn@Co@CN, and (d) ZnSe@CoSe for sodium-ion storage, respectively.

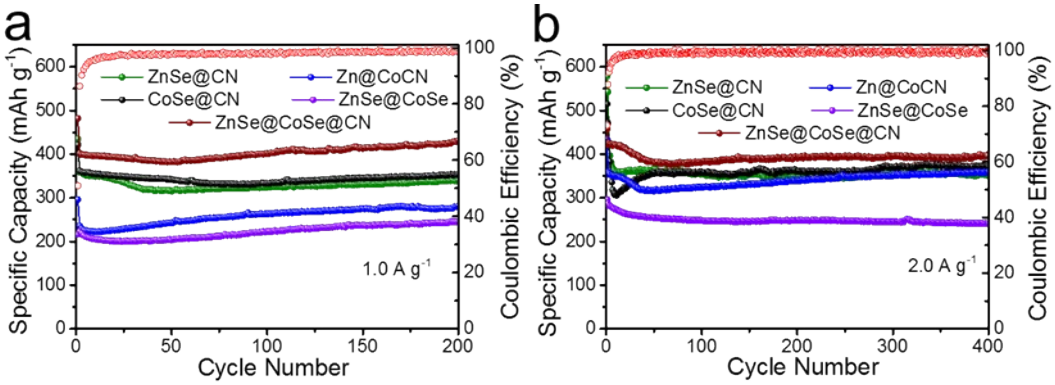

Figure S15. Cycling performance of the anodes at (a) 1.0 A g^{-1} and (b) 2.0 A g^{-1} for sodium-ion storage.

Table S1. XPS measured element contents of the samples.

Samples	C[atomic%]	N[atomic%]	O[atomic%]	Co[atomic%]	Zn[atomic%]	Se[atomic%]
ZnSe@CN	68.98	9.64	16.46	—	2.26	2.74
CoSe@CN	68.47	8.05	19.31	1.69	—	2.47
Zn@Co@CN	75.82	9.4	12.57	1.06	1.11	—
ZnSe@CoSe	68.99	11.06	13.06	1.8	1.68	3.41
ZnSe@CoSe@CN	72	10.55	11.87	1.14	1.15	3.29

Table S2. The specific surface area and total pore volume of the samples.

Samples	Surface area ($m^2 \cdot g^{-1}$)	Total pore volume ($cm^3 \cdot g^{-1}$)
ZnSe@CN	120.61	2.892
CoSe@CN	143.89	3.555
Zn@Co@CN	275.49	5.693
ZnSe@CoSe	191.267	4.724
ZnSe@CoSe@CN	168.81	4.454

Table S3. Electrochemical performances of the anode materials for lithium-ion storage.

	Materials	Current density (mAh g^{-1})	Initial Discharge Capacity (mAh g^{-1}) / Initial Charge Capacity (mAh g^{-1})	ICE(%)	Reversible Capacity (mAh g^{-1}) after (Cycle number) at current density (mAh g^{-1})	Reference
Performance of LIB	**ZnSe@CoSe@CN**	**100**	**2839 / 1443**	**50.84**	**1567 (100) (100)**	**This work**
		1000	**1887 / 1016**	**53.85**	**1087 (200) (1000)**	
		2000	**1091 / 604**	**55.2**	**870 (400) (2000)**	
		5000	**1255 / 641**	**51.1**	**568 (1000) (5000)**	
	ZCS@NC/CNTs	100	1182 / 691	58.4	873 (500) (500)	[S1]
					406 (1000) (1000)	
	$CoSe_2$-decorated $NbSe_2$	100	1187 / 665	56	364 (1500) (5000)	[S2]
	ZnSe/$CoSe_2$@N–C	100	1274 / 866	67.9	436 (113) (2000)	[S3]
					966 (500) (2000)	
	$CoSe_2$@C/CNTs	1000	687 / 562	81.8	606 (100) (100)	[S4]
					428 (500) (1000)	
	ZnSe/CoSe/NC DPH	100	1616 / 977	60.4	1216(100) (100)	[S5]
					515 (100) (1000)	
	ZnSe@C	100	869 / 660	75.9	712 (100) (100)	[S6]
					617 (800) (1000)	
					472 (800) (2000)	
	ZnCoO/C (2:1)	100	1371 / 1206	88	1050 (300) (100)	[S7]
					711 (500) (1000)	
	HCN	200	1350 / 806	58.2	963 (100) (200)	[S8]
					561 (1000) (1000)	
					374 (5000) (5000)	

Table S4. Electrochemical performances of the anode materials for sodium-ion storage.

	Materials	Current density ($A\ g^{-1}$)	Initial Discharge Capacity ($mAh\ g^{-1}$) / Initial Charge Capacity ($mAh\ g^{-1}$)	ICE(%)	Reversible Capacity ($mAh\ g^{-1}$) after (Cycle number) at current density ($A\ g^{-1}$)	reference
Performance of SIB	**ZnSe@CoSe@CN**	**0.1**	**660 / 559**	**84.6**	**591(100) (0.1)**	**This work**
		1.0	**481 / 245**	**50.92**	**431 (200) (1.0)**	
		2.0	**457 / 335**	**73.18**	**397 (400) (2.0)**	
		5.0	**587 / 499**	**85**	**390 (1000) (5.0)**	
	$ZnSe/CoSe_2/C$	0.2	846 /475	56.1	475 (120) (0.2)	[S9]
					363 (400) (1.0)	
					239 (500) (5.0)	
	$ZnSe/2(CoSe_2)/NC$	0.1	857 / 537	62.7	552 (100) (0.1)	[S10]
					395 (500) (1.0)	
	$In_2Se_3/CoSe_2$	0.1	827 / 506	61.2	445 (200) (0.5)	[S11]
					297 (2000) (5.0)	
	NCNF@MoSSe	1.0	823 / 495	60.1	416 (100) (1.0)	[S12]
					323 (700) (2.0)	
	$CNT/CoSe_2/C$	0.1	952 / 544	57.1	531 (100) (0.1)	[S13]
					396 (300) (0.5)	
	HCN	0.1	504 / 340	67.5	351 (500) (0.1)	[S8]
					213 (1000) (1.0)	
					154 (1000) (5.0)	
	$ZnSe\subset N\text{-}C@MoSe_2/rGO$	1.0	675 / 350	51.85	319 (1800) (1.0)	[S14]
					301 (1100) (2.0)	
					238 (1500) (5.0)	
	$CoSe_2/CNFs$	0.2	972 / 516	53	430 (400) (0.2)	[S15]
					370 (1000) (2.0)	
	$MoSe_2@CoSe/N\text{-}C$	0.1	557 / 452	81.1	485 (100) (0.1)	[S16]
					347 (300) (2.0)	
	Zn-Co-Se@NDC	0.2	550 / 506	87	446 (200) (0.2)	[S17]
					344 (2000) (5.0)	

References

[S1] J. Jin, Y. Zheng, L. B. Kong, N. Srikanth, Q. Y. Yan and K. Zhou, *J. Mater. Chem. A*, 2018, **6**, 15710-15717.

[S2] J. L. Zhang, C. F. Du, J. Zhao, H. Ren, Q. H. Liang, Y. Zheng, S. Madhavi, X. Wang, J. W. Zhu and Q. Y. Yan, *ACS Appl. Mater. Interfaces*, 2018, **10**, 37773-37778.

[S3] Q. Liu, J. G. Hou, Q. Hao, P. Huang, C. X. Xu, Q. X. Zhou, J. Zhou and H. Liu, *Nanoscale*, 2020, **12**, 22778-22786.

[S4] J. Yang, H. Gao, S. Men, Z. Shi, Z. Lin, X. Kang and S. Chen, *Adv. Sci.*, 2018, **5**, 1800763.

[S5] H. D. Liu, Y. Lin, M. N. Li, L. Zhang, Y. Lu and W. Xiao, *Int. J. Hydrog. Energy*, 2021, **46**, 30818-30827.

[S6] D. J. Ma, Q. L. Zhu, X. T Li, H. C. Gao, X. F. Wang, X. W. Kang and Y. Tian, *ACS Appl. Mater. Interfaces*, 2019, **11**, 8009-8017.

[S7] B. Joshi, E. Samuel, Y. I. Kim, G. Periyasami, M. Rahaman and S. S. Yoon, *J. Mater. Sci Technol.*, 2021, **67**, 116-126.

[S8] Z. Zhang, Y. Huang, X. Li, S. Zhang, Q. X. Jia and T. H. Li, *Chem. Eng. J.*, 2021, **421**, 129827.

[S9] S. Y. Jeong and J. S. Cho, *Nanomaterials Basel*, 2019, **9**, 1362.

[S10] P. Liu, J. Han, K. Zhu, Z. Dong and L. Jiao, *Adv. Energy Mater.*, 2020, **10**, 2000741.

[S11] S. H. Xiao, X. Y. Li, W. S. Zhang, Y. Xiang, T. S. Li, X. B. Niu, J. S. Chen and Q. Y. Yan, *ACS Nano*, 2021, **15**, 13307-13318.

[S12] J. W. Shi, H. Li, Y. W. Liu, Q. Y. Lu and F. Gao, *Adv. Mater. Interfaces*, 2022, **9**, 2102408.

[S13] M. Yousaf, Y. J. Chen, H. Tabassum, Z. P. Wang, Y. S. Wang, A. Y. Abid, A. Mahmood, N. Mahmood, S. J. Guo, R. P. S. Han and P. Gao, *Adv. Sci.*, 2020, **7**, 1902907.

[S14] N. X. Shi, Y. T. Chu, B. J. Xi, M. Huang, W. H. Chen, B. Duan, C. H. Zhang, J. K. Feng and S. L. Xiong, *Adv. Energy Mater.*, 2020, **10**, 2002298.

[S15] H. Yin, H. Q. Qu, Z. T. Liu, R. Z. Jiang, C. Li and M. Q. Zhu, *Nano Energy*, 2019, **58**, 715-723.

[S16] J. Chen, A. Q. Pan, Y. P. Wang, X. X. Cao, W. C. Zhang, X. Z. Kong, Q. Su, J. D. Lin, G. Z. Cao and S. Q. Liang, *Energy Stor. Mater.*, 2019, **21**, 97-106.

[S17] J. Feng, S. H. Luo, S. X. Yan, Y. Zhan, Q. Wang, Y. H. Zhang, X. Liu and L. J. Chang, *Small*, 2021, **17**, 2101887.